The synaptonuclear messenger RNF10 acts as an architect of neuronal morphology

Nicolò Carrano[1†], Tanmoy Samaddar[1†], Electra Brunialti[1], Luca Franchini[1], Elena Marcello[1], Paolo Ciana[2], Daniela Mauceri[3], Monica Di Luca[1] and Fabrizio Gardoni[1*]

[1]Department of Pharmacological and Biomolecular Sciences, University of Milan, Via Balzaretti 9, 20133 Milan, Italy.
[2]Department of Oncology and Hemato-Oncology, University of Milan, Via Balzaretti 9, 20133 Milan, Italy.
[3]Department of Neurobiology, Interdisciplinary Centre for Neurosciences [IZN], Heidelberg University, INF 366 69120 Heidelberg, Germany.

[†]These authors contributed equally to this work and are listed alphabetically

[*]Corresponding author: Fabrizio Gardoni, Department of Pharmacological and Biomolecular Sciences, Università degli Studi di Milano, Via Balzaretti 9, 20133, Milan, Italy. Tel: +39-0250318374/314; Email: fabrizio.gardoni@unimi.it

ABSTRACT

The Ring Finger Protein 10 [RNF10] is a novel *synapse-to-nucleus* signaling protein that specifically links activation of synaptic NMDA receptors to modulation of gene expression. RNF10 dissociation from the GluN2A subunit of the NMDA receptor represents the first step of its synaptonuclear transport and it is followed by an importin-dependent translocation into the nucleus. Here we have identified protein kinase C [PKC]-dependent phosphorylation of RNF10 Ser31 as a key step for RNF10 detachment from NMDA receptor and its subsequent trafficking to the nucleus. We show that pSer31-RNF10 plays a role both in synaptonuclear signaling and in neuronal morphology. In particular, the prevention of Ser31 RNF10 phosphorylation induces a decrease in spine density, neuronal branching and CREB signaling, while opposite effects are obtained by mimicking a stable RNF10 phosphorylation at Ser31. Overall, these results add novel information about the functional and structural role of synaptonuclear protein messengers in shaping dendritic architecture in hippocampal neurons.

KEYWORDS

NMDA receptor, synaptonuclear messenger, phosphorylation, dendritic arborization, hippocampus.

INTRODUCTION

The active communication between synapses and the nucleus is needed for long-term functional regulation of neuronal activity as well as for shaping neuronal morphology [1]. In the last decade an increasing number of synaptonuclear protein messengers have been identified and characterized [2-5]. Overall these studies have clearly demonstrated that a correct functioning of synaptonuclear messengers represents a key element in the modulation of synaptic transmission at excitatory synapses [3,6]. On the other hand, alterations of synaptonuclear messengers' activity have been correlated to synaptic failure as observed in different synaptopathies, including both neurodevelopmental disorders and neurodegenerative diseases [6].

The activation of NMDA-type glutamate receptors (NMDARs) is of primary importance in these events [4]. On this line, we have recently identified Ring Finger Protein 10 (RNF10) as a novel synaptonuclear signaling protein that specifically links activation of synaptic GluN2A-containing NMDARs to nuclear gene expression [7]. RNF10 moves to the nucleus after synaptic GluN2A-containing NMDARs activation and induction of long-term potentiation (LTP), regulating the expression of specific target genes, as $p21^{WAF1/cip1}$ [8,9]. Conversely, induction of long-term depression (LTD) does not modify RNF10/GluN2A interaction and RNF10 nuclear trafficking [7]. Notably, RNF10 is responsible for long-lasting re-shaping of dendritic spines as required to convey LTP expression [7]. RNF10 dissociates from the GluN2A subunit of the NMDAR complex in an activity-dependent manner and we provided compelling evidence for importin-dependent long-distance transport from synapto-dendritic compartments to the nucleus [7]. However, the molecular mechanism/s leading to NMDAR/RNF10 complex disruption and for initiating the importin-mediated trafficking of RNF10 to the nucleus remain unclear.

Here, we describe a protein kinase C (PKC)-dependent phosphorylation event on RNF10 (Ser31) which drives RNF10 synaptonuclear trafficking. Moreover, we provide compelling evidence that pSer31-RNF10 plays a key role in activation of plasticity-related signaling pathways, as pCREB induction, neuronal arborization and dendritic spines density in hippocampal neurons.

MATHERIALS AND METHODS

Primary hippocampal neurons and COS-7 cells

Hippocampal neuronal cultures were prepared from embryonic day 18-19 (E18-E19) rat hippocampi as described previously [8]. Neurons were transfected between DIV7-DIV10 using the calcium phosphate method. COS-7 cells were maintained in DMEM + Glutamax medium (GIBCO-BRL) supplemented with 10% Fetal Bovine Serum (FBS; GIBCO-BRL) and Pen/Strep (GIBCO-BRL). The day prior to

transfection, the cells were plated in 6 wells multiwell plates (for biochemistry) or on coverslips in 12 wells multiwell plates (for immunostaining). Cells were transfected using the lipofectamine method (Invitrogen; Carlsbad, CA, USA). Cells were lysed or fixed for immunostaining after 36h.The procedures on rats were carried out according to the European Communities Council Directive 2010/63/EU and the current Italian Law on the welfare of the laboratory animal (D.Lgs. n.26/2014). Institutional Animal Care and Use Committee of University of Milan and by the Italian Ministry of Health (#326/2015) approved all the experiments involving primary neuronal cultures preparation.

Subcellular fractionation

Neurons were lysed in a buffer containing 0.32 M Sucrose, 1 mM Hepes, 1 mM NaF, 0.1 mM PMSF, 1 mM MgCl using a glass-glass homogenizer. To purify post-synaptic triton insoluble fractions (TIF) [9], lysates were centrifuged at 1,000 g for 5 min at 4°C. The supernatant was centrifuged at 13,000 g for 15 min at 4°C. The pellet was dissolved in a buffer containing 0.5% Triton and 150 mM KCl, incubated on ice for 15 min and centrifuged at 100,000 g for 1 h at 4°C. The resulting pellet (TIF) was homogenized by passing through a 1ml hypodermic syringe in 20mM HEPES buffer. To prepare a crude nuclear fraction, the lysates were centrifuged at 1,000 g for 10 min and the pellet was dissolved in 20mM HEPES buffer. Crude membrane fractions were tested for the almost complete absence of synaptic proteins (GluN2A, GluA1, PSD-95) and the enrichment in nuclear proteins (Histone H3; see Fig. A1). All steps were done in presence of protease inhibitors (Complete^{TM}, GE Healthcare, Mannheim, Germany) and phosphatase inhibitors (PhosSTOP^{TM}, Roche Diagnostics GmbH, Mannheim, Germany). Protein content of the samples has been quantified by using the Bio-Rad protein assay reagent (Hercules, CA, USA) and equivalent amounts of proteins loaded in individual lanes for western blot analysis.

Cloning, expression, and purification of glutathione S-transferase [GST] fusion protein

Point mutations were generated in the RNF10 sequence either in the pGEX-KG, dtEOS, GFP-tag or Myc-tag vectors, using primers designed to create a missense mutation in a PCR reaction using Pfu polymerase (Stratagene). GST-RNF10 fusion proteins containing wild-type or mutated RNF10 were expressed in *Escherichia coli* and purified on glutathione agarose beads (Sigma Aldrich, St. Louis, MO) as previously described [12].

The p21prom-Luc2-T2A-tdTomato reporter system was created by cloning 4.5 Kb promoter region of the mouse p21waf1/cip1 gene upstream a bicistronic reporter system containing the luc2 [10] and td-Tomato [11] genes joined by the T2A self-cleaving peptide sequence. The 4.5 Kb promoter region was amplified with Platinum™ Pfx DNA Polymerase (Thermo Fisher Scientific) from genomic DNA using the following primers:

m_p21_3b_for 5'-GGATTCGCATATGGCAGATCCACAGCGATATCC-3'

m_p21_4530a_rev 5'-CTGGTCAGTCGACCATGGTGCCTGTGGCTGAAA-3'

Co-immunoprecipitation assays [co-i.p.]

Homogenate/TIF aliquots containing 150 μg/50 μg of proteins were incubated overnight at 4°C with primary antibody in RIPA buffer containing 50 mM Tris HCl (pH 7.2), 150 mM NaCl, 1% NP-40, 0.5% deoxycholic acid, 0.2% sodium dodecyl sulphate (SDS). As control, one sample was incubated in the same experimental conditions without the antibody or without any homogenate/TIF added. Protein A/G-sepharose beads (Sigma-Aldrich) were added and incubated for additional 2 h, at room temperature, on a rotator. Beads were precipitated by mild centrifugation, washed three times with RIPA buffer containing 0.1% SDS and boiled for 10 min in SDS-PAGE sample buffer. Beads were precipitated using centrifugation and the supernatant loaded onto SDS-PAGE gels. For the input lane, 10% of the Homogenate/TIF aliquot used for the co-i.p. experiment was loaded onto the SDS-PAGE.

Pull-down assay

Neuronal homogenates containing 250 μg of proteins were incubated at room temperature with GST-beads to a final volume of 1 ml with Tris Buffered Saline (TBS) solution for 1h on an eppendorf rotator. The GST-beads were precipitated by centrifugation and the supernatant re-incubated at room temperature with GST fusion proteins or GST alone, for an additional 2h on a rotator. Beads were precipitated and washed three times with TBS containing 0.1% Triton X-100. Beads were boiled in SDS-PAGE sample buffer, loaded onto SDS-PAGE gels and analyzed by western blotting.

Luciferase assays

The 5HRp21_Luc2_T2A_TdTomato luciferase reporter plasmid was co-transfected in primary hippocampal neurons with a plasmid containing an expression cassette for *Renilla* luciferase for normalization with or without either RNF10wt, RNF10S31D or RNF31S31A. Neurons were harvested 4 days post-transfection. Luciferase activities were measured with the Dual-Glo Luciferase assay kit (Promega) following manufacturer's instructions. Data derive from three independent experiments, each performed with technical duplicates.

Confocal imaging

Primary hippocampal neurons were treated at *DIV14* and fixed with 4% PFA- 4% sucrose at 4°C for 5 mins followed by washes with PBS. The cells were next permeabilized with 0.2% Triton-X100 in PBS and blocked with 5% BSA in PBS for 1 h at room temperature. Primary antibodies in 3 % BSA in PBS was used to incubated overnight at 4°C chamber in a humidified chamber followed by extensive washing with PBS at room temperature. Secondary antibodies were applied in 3% BSA in PBS, washed in PBS and mounted on slides with Fluoroshield mounting medium (Sigma). Fluorescence images were acquired

by using Zeiss Confocal LSM510 system or Nikon A1 Ti2 system with a sequential acquisition setting at 1024x1024 pixels resolution; cells were selected from different coverslips at random for quantification. For co-localization studies the signals for each image were kept within the linear range and settings were consistent between different experimental conditions for an unbiased comparison. Proximity Ligation Assay (PLA) was performed as previously described [7]. After fixation, incubation with blocking solution and permeabilization, cells were incubated with mouse monoclonal anti-Myc antibody (1:2000; Millipore) and rabbit polyclonal anti- GluN2A antibody (1:200; Lifetechnologies) or anti-RNF10 antibody (1:200; Proteintech) and anti-GluN2A antibody (1:200; Neuromab) overnight at 4°C in a humidified chamber. After washes with PBS, cells were incubated for 1h with the PLA secondary probes anti-mouse Plus and anti-rabbit Minus (Olink Bioscience) at 37°C. Cells were washed thrice with Duolink II Wash Buffer A (Olink Bioscience) and incubated with the ligation in ligase buffer [Olink Bioscience] for 30 min at 37°C. After two additional rinsing with Wash Buffer A, cells were incubated with DNA polymerase (1:80; Olink Bioscience) in the amplification buffer (Olink Bioscience) for 100 min at 37°C in dark. Cells were next washed with Duolink II Wash Buffer B (Olink Bioscience) and then, if necessary, incubated with chicken polyclonal anti-GFP (1:400; Milipore) overnight at 4°C. After washing with PBS, cells were incubated with secondary goat anti-chicken-AlexaFluor 488 for 1h at room temperature. The cells were washed in PBS and mounted on slides with Fluoroshield mounting medium (Sigma).

Zeiss Confocal LSM510 system was used for time-lapse imaging of RNF10 fused to tdEOS. For the photoconversion of tdEOS, ROIs were selected along distal dendrites and then 405 nm stimulation at 50% laser power was applied. Along the z-axis at list 10 optical sections with focus depth of 300-400 nm were taken in order to cover the complete volume of imaged neurons. Neurons were imaged for 42 minutes under controlled temperature and CO_2 levels.

For three-dimensional morphological Sholl analysis, total dendritic length and dendrite morphology were calculated by using Fiji freeware software with the Simple Neurite Tracer plug-in. Briefly, a z-stack acquisition was imported, calibrated in Fiji, and semi-automatically traced. Total dendritic length was then computed. The shell interval was set at 5 μm. All analyses were performed blind. In all the experiments, for each condition, a minimum of 5 neurons from 3 independent preparations was analyzed. For spine density analysis, Fiji freeware software was used. Stacks were projected along the z axis to obtain an image with all the spines in focus. Spines were counted and then dendrite length measured with the segmented line function of FIJI.

Drug treatments

Synaptic stimulation (SynStim) was performed treating neurons at *DIV14* with bicuculline (50 μM; Tocris), 2,5 mM 4-aminopyridine (4-AP; Tocris) and 5 μM ifenprodil in Neurobasal medium supplemented with B27 for 30 min as previously reported [7]. Chemical LTP (cLTP) protocol was performed as previously reported [7,12]. Briefly, neurons were incubated in artificial cerebrospinal fluid (ACSF, 125mM NaCl, 25mM KCl, 2 mM $CaCl_2$, 33 mM Glucose and 25 mM HEPES) + 1 mM $MgCl_2$ for 30 minutes at 37°C, then cLTP induction was performed in ACSF without $MgCl_2$, plus 50 μM Forskolin (Tocris), 0.1 μM Rolipram (Tocris) and 100 μM Picrotoxin (Tocris) for 16 minutes. Control groups were kept in normal ACSF. Bisindolylmaleimide I (BIM, 10 μM; Tocris) or Autocamtide II-related inhibitory peptide (10 nM, Calbiochem) were incubated for 10 min followed by the SynStim protocol for 30 min (post-translational effect) or 2h (transcriptional effect). Phorbol 12-myristate 13-acetate (PMA, 10 μM; Tocris) was incubated in Neurobasal medium supplemented with B27 for 15 minutes at 37°C.

Antibodies

The following antibodies were used: monoclonal antibody (mAb) anti-α-calcium/calmodulin-dependent kinase II (αCaMKII), polyclonal antibody (pAb) anti-GluN2A, pAb anti-CREB, pAb anti-p-CREB (Ser-133) and mAb anti-Myc were purchased from Millipore (Billenca, MA, USA); mAb anti-Meox2 was purchased from Abcam (Cambridge, MA, USA); pAb anti-p44/42 MAPK, pAb anti-p-p44/42 MAPK (Thr202/Tyr204) were purchased from Cell Signalling (Danvers, MA, USA); mAb anti-GFP, mAb anti-GST and anti-PSD-95 were purchased from NeuroMab (Davis, CA, USA); mAb anti-alpha-Tubulin and mAb anti-Flag were purchased from Sigma-Aldrich (St. Louis, MO, USA); mAb anti-p21 were purchased from BD Biosciences (NJ); pAb anti-histone H3 and pAb anti-RNF10 were purchased from Proteintech (Chicago, MI, USA, USA); mAb anti-JL8 was purchased from Clontech (Mountain View, CA, USA); pAb anti-HA was purchased from Santa Cruz Biotechnology (Dallas, TX, USA) p-RNF10(S31) was custom generated from Primm (Cambridge, MA, USA). Peroxidase-conjugated secondary anti-mouse Ab and peroxidase-conjugated secondary anti-rabbit Ab was purchased from Bio-Rad (Hercules, CA, USA). AlexaFluor secondary Abs were purchased from Invitrogen (Carlsbad, CA, USA).

Statistical analysis

Statistical analysis was performed with GraphPad Prism6 software. The tests used to assess data significance are indicated in the figure legends. For WB, IP and GST-pulldown assay, at least 3 independent experiments were performed. For confocal studies, at least 10 neurons coming from 3 different experiments were analyzed. Data are presented as mean ± SEM.

RESULTS

PKC activation regulates RNF10 translocation to the nucleus

RNF10 association with the NMDAR complex is strictly dependent on the interaction between RNF10 N-terminal domain (aa 1-74) and the C-tail of the GluN2A subunit [7]. Of note, calcium significantly reduces the formation of GluN2A/RNF10 complex by promoting the association of calmodulin (CaM) at the same GluN2A binding site [7]. Bioinformatic tools (NetPhos 3.1, KinasePhos 2.0, phosphosite.org) indicated the presence of several putative PKC-dependent phosphosites within the RNF10 sequence aa 1-74 (Fig A2). Thus, we sought to investigate the possible role of PKC in the disruption of RNF10/NMDAR complex and RNF10 trafficking to the nucleus. We have previously demonstrated that stimulation of synaptic NMDARs induces RNF10 synaptonuclear trafficking leading to its nuclear accumulation [7]. To characterize the role of PKC in the modulation of RNF10 trafficking induced by activation of the excitatory synapse, NMDAR synaptic stimulation was applied in primary hippocampal cultures in presence or absence of a highly selective, cell-permeable and reversible PKC inhibitor (Bisindolylmaleimid; BIM) [13]. Proximity Ligation Assay (PLA) experiments revealed that synaptic stimulation of NMDAR induces a significant reduction of the interaction between RNF10 and GluN2A, as a lower number of PLA clusters was detected compared to the control (Fig 1a). BIM co-incubation fully prevented the synaptic stimulation-induced loss of interaction between RNF10 and GluN2A (Fig 1a). Moreover, confocal imaging (Fig 1b) and western blotting analyses performed in crude nuclear extracts (Fig 1c) indicate that BIM completely prevented the expected RNF10 nuclear accumulation induced by activation of synaptic NMDARs. Further, PKC inhibitor also blocked the synaptic stimulation-mediated up-regulation of $p21^{WAF1/Cip1}$ protein levels (Fig 1d), a well-validated target gene of the RNF10 pathway [7,14,15]. Conversely, inhibition of another NMDAR-associated kinase such as CaMKII [16], did not block RNF10 nuclear accumulation induced by synaptic stimulation of NMDAR (Fig A3).

In addition, treatment of primary hippocampal neurons with the PKC activator phorbol 12-myristate 13-acetate (PMA; 10 μM) [17] led to an increase of RNF10 nuclear levels measured by confocal imaging (Fig 1e) and western blotting analyses of crude nuclear fractions (Fig 1f). Taken together, these results indicate that PKC activation is essential for the induction of RNF10 translocation to the nucleus and modulation of the expression of RNF10 target genes.

RNF10 phosphorylation by PKC modulates RNF10/NMDAR complex dissociation and nuclear localization

In order to confirm that PKC-dependent modulation of RNF10 trafficking is directly correlated to a kinase-substrate event, we analyzed RNF10 phosphorylation in primary hippocampal neurons following synaptic stimulation in presence or absence of the PKC inhibitor. Neuronal homogenates were immunoprecipitated using an anti-phospho-serine antibody. Western blotting analysis of RNF10 revealed an increase of RNF10 phosphorylation on serine residues following stimulation of synaptic NMDARs in the immunocomplex (Fig 2a). The PKC inhibitor fully prevented RNF10 serine phosphorylation, suggesting that PKC is the main kinase involved in the process (Fig 2a). Analysis of RNF10(1-74) domain (see Fig A2) revealed the presence of at least four serine residues (Ser5, Ser31, Ser39, Ser70) that might represent a putative phosphate acceptor site for PKC and possibly involved in the regulation of RNF10 binding to GluN2A. A point mutation strategy was used to determine the effects of PKC site-specific phosphorylation of RNF10. GST fusion proteins of RNF10(1-74) wild-type (wt) and with single Ser/Asp mutation, mimicking the phosphorylation, were generated and used in an *in vitro* pull-down assay from rat hippocampal homogenates. As shown in Fig 2b, Ser31Asp (S31D) mutation completely abolished the capability of GST-RNF10 fusion protein to bind the GluN2A subunit. No significant difference in RNF10's ability to form the GluN2A/RNF10 complex was observed by using S5D, S39D and S70D constructs compared to the wild type counterpart (Fig 2b).

We then transfected COS-7 cells with GFP-GluN2A and Myc-RNF10wt, Myc-RNF10S31D (mimicking phosphorylation) or Myc-RNF10S31A [not permissive of phosphorylation as control). A co-immunoprecipitation assay was performed in cell lysates to confirm the role of RNF10 Ser31 phosphorylation in the modulation of RNF10 interaction with the NMDAR subunit. No effect was observed by the S31A mutation (Fig 2c). Conversely, S31D mutation induced a significant reduction of RNF10 binding to GluN2A (Fig 2c). These results confirm that also in a heterologous system the phosphorylation of Ser 31 residue interferes with the formation of GluN2A/RNF10 complex (Fig 2c). In addition, no effect of S31D and S31A mutations on RNF10 interaction with importin1α was observed (Fig A4) [7], thus suggesting that Ser31 phosphorylation does not affect importin-mediated trafficking of RNF10 to the nucleus [7].

To unravel the functional significance of PKC-dependent phosphorylation of RNF10 in hippocampal neurons, a phosphospecific antibody – RNF10S31P – was produced, affinity purified and characterized (see Fig A5). RNF10S31P antibody recognized with higher affinity the purified GST-RNF10S31D mutated fusion protein, mimicking the phosphorylation, compared to GST-RNF10WT (Fig A5a). Further, the RNF10S31P antibody detected myc-RNF10S31D but not myc-RNF10S31A in lysates derived from transfected COS-7 cells (Fig A5b). Finally, we infected primary hippocampal neurons with either the LKO-shRNF10 lentivirus targeting RNF10 expression or scrambled sequence as a control.

RNF10 silencing via shRNF10 lentivirus significantly reduced the RNF10 protein level compared to scramble construct as previously demonstrated [7]. No signal was detected in the shRNF10 sample both using the commercial RNF10 antibody and the custom made RNF10S31P (Fig A5c).

Western blotting analysis for RNF10S31P in primary hippocampal neurons revealed an increase of RNF10 Ser31 phosphorylation in postsynaptic membrane fractions (triton insoluble fractions – TIF) following synaptic stimulation of NMDAR (Fig 2d) in agreement with the results observed using the pan-phosphoserine antibody (Fig 2a). PKC inhibitor completely prevented Ser31 phosphorylation (Fig 2d). Similarly, also a highly validated protocol to induce cLTP [7,12] was sufficient to increase RNF10 Ser31 phosphorylation as measured 15 minutes after cLTP induction (Fig 2e). We used two different experimental approaches to monitor if RNF10 accumulated in the nucleus after synaptic stimulation remains phosphorylated on Ser31. Western blotting analysis for RNF10S31P revealed an increase of RNF10 Ser31 phosphorylation in the crude nuclear fraction following synaptic stimulation of NMDAR (Fig. 2f, left graph). However, considering the above-described accumulation of RNF10 in the nucleus after synaptic stimulation (see Fig. 1b,c), we didn't observe any increase of the PSer31-RNF10/total RNF10 ratio (Fig. 2f, right graph). To better address this issue, we performed PLA experiments using the RNF10S31P antibody and total RNF10 antibody for the assay. As shown in Fig. 2g, we found a significant increase of nuclear PLA clusters indicating Ser31 phosphorylation following stimulation of synaptic NMDARs (Fig. 2g).

To demonstrate that Ser31 phosphorylation controls the synaptic stimulation-induced RNF10 translocation from the synapse to the nucleus, we used a live imaging approach based on TdEOS plasmid. TdEOS is a bright and photostable photoconvertible fluorescent tag that after stimulation changes its emission wavelength from green to red allowing the tracking of the movement of the labeled protein into biological systems [5,7]. We monitored the nuclear translocation of RNF10 WT-tdEOS and the RNF10 S31A-tdEOS mutant by confocal imaging following synaptic stimulation. As expected [7], after photoconversion in distal dendrites, RNF10 WT moved from the synapse to the nucleus in synaptic stimulation conditions (Fig 3a). Photoconverted RNF10S31A mutant did not accumulate into the nucleus (Fig 3a), confirming that RNF10 Ser31 phosphorylation is key for the dissociation from GluN2A and the subsequent nuclear trafficking. We confirmed the specific role of Ser31 phosphorylation in the modulation of RNF10 clustering with GluN2A by PLA in primary hippocampal neurons transfected with GFP-GluN2A and either Myc-RNF10WT or Myc-RNF10S31D. A significant lower number of PLA signals were detected for the S31D construct indicating a decreased number of RNF10 molecules in close proximity (<40 nm) to the receptor subunit (Fig 3b). In addition, immunofluorescence on primary hippocampal neurons transfected with Myc-RNF10WT or Myc-RNF10S31D revealed that Myc-

RNF10S31D spontaneously accumulated in the nucleus in absence of any stimulation (Fig 3c), compared to Myc-RNF10WT that localized more in the cytosolic compartment, as previously reported [7].

To assess whether the Ser31 phosphorylation-triggered RNF10 translocation to the nucleus affects gene expression, we performed a luciferase assay on primary hippocampal neurons transfected with a reporter construct expressing the firefly luciferase under the promoter of the validated RNF10 target $p21^{WAF1/cip1}$ (5HRp21_Luc2_T2A_TdTomato, see methods) [7,15]. Neurons were transfected with RNF10WT, RNF10S31A or RNF10S31D together with the luciferase reporter and normalizer (*Renilla* luciferase) constructs. As expected, RNF10S31D expression was associated to a higher firefly luciferase activity (Fig 3d), indicative of a higher transcriptional activity induced by the mutant. RNF10S31A did not show difference in comparison to control (Fig 3d).

The modulation of RNF10 activity results in the alteration of neuronal morphology

We previously reported the role of RNF10 in implementing LTP-mediated cellular effects and LTP maintenance [7]. Since Ser31-mediated nuclear accumulation affects the functionality of RNF10, we investigated whether manipulations of Ser31 phosphorylation could affect the capacity of RNF10 to convey LTP signaling pathways. We used CREB phosphorylation as a marker for the synaptic activation of NMDAR and plasticity [18-24]. RNF10S31A transfected neurons had a decreased amount of pCREB levels compared to control, while RNF10S31D was able to induce pCREB expression (Fig 4a). Taken together, our results suggest that the phosphorylation state of Ser31 on RNF10 is key for its nuclear accumulation and for signaling events downstream of NMDAR activation.

We previously found that RNF10 downregulation was associated to a decreased number of dendritic spines in hippocampal neurons [7]. Interfering with the expression of RNF10 via shRNA-mediated silencing (shRNF10), induced a significant simplification of dendrite arborization in primary hippocampal neuronal cultures in comparison to controls suggesting that RNF10 might have a global effect on dendritic architecture (Fig 4c). We analyzed if RNF10 Ser31 phosphorylation state could regulate spine density and dendritic geometry. Morphometric analyses of primary hippocampal neurons transfected with RNF10WT, RNF10S31A and RNF10S31D showed that RNF10S31A mutant induced a severe reduction of spine number (Fig 4b) thus acting as a dominant negative protein. RNF10S31D had the opposite effect (Fig 4b). No effect on spine density was observed following overexpression of RNF10WT, suggesting that a strong activation of a PKC-RNF10Ser31 dependent pathway, as for RNF10S31D, is needed for an increase of spine density (Fig 4b). Notably, RNF10S31A expression reduced also dendritic arbor complexity compared to control (Fig 4d). RNF10WT and RNF10S31D, on the contrary, did not alter neuronal geometry.

Taken together these results show that RNF10 functioning, encoded by its Ser31 phosphorylation, is necessary for the regulation of dendritic spines number and dendritic arborization.

DISCUSSION

Synaptonuclear protein messengers (i.e. Jakob, Abi-1 and CRTC1) represent a fundamental player for the regulation of neuronal morphology both in health and diseases [6]. Accordingly, Jacob KO mice show hippocampal dysplasia with a reduced number of synapses and dendritic branching [25], Abi-1 silencing leads to aberrant dendrite branching and decreased spine density, whereas Abi-1 overexpression shows opposite effects [26]. Finally, CRTC1 plays a key role BDNF-induced dendritic development [27,28]. Elaborated branched structures are indeed a key requirement to maintain a correct synaptic capacity; on the other hand, the transcriptional regulation of gene expression has been proven as an asset in dictating neuronal architecture in an activity dependent manner.

Here, we demonstrate that RNF10 silencing as well as inhibition of RNF10 nuclear trafficking lead to a dramatic alteration of neuronal morphology and function with reduced dendritic branching, spine loss and a decrease in pCREB signaling. This effect is specifically linked to activation of the synaptic pool of NMDARs. In particular, we demonstrate that activation of synaptic NMDARs or induction of cLTP lead to RNF10 phosphorylation by PKC and its translocation to the nucleus and that this event is involved in neuronal branching.

We identified a specific PKC-dependent mechanism, namely RNF10 phosphorylation in Ser31, as the key driver needed for RNF10 dissociation from synaptic NMDARs and consequent trafficking to the nucleus. Previous studies demonstrated that NMDAR-mediated activity enhances dendritic arborization by modulating among others RhoA, Rac and Cdc42 activity [29,30] and it is key for the maintenance of established dendritic trees [31]. More recent evidences correlated NMDAR activity to the induction of neuronal branching [32] addressing also the putative role of each regulatory GluN2-type subunits in these events [33,34]. GluN2A silencing reduces branch clusters [33] and decreased total dendritic length and dendritic complexity in hippocampal neurons [34].

Several publications demonstrated that NMDAR functions are strictly regulated by PKC [35-38]. Early reports demonstrated that PKC phosphorylates NMDARs at different sites [35,36] and clearly indicated the existence of a PKC-dependent potentiation of NMDAR activity playing a role in NMDAR-dependent plasticity [37,38]. However, PKC-induced potentiation of NMDAR activity does not probably occur by direct phosphorylation of the receptor protein but rather of associated signaling proteins [39]. Here we show that activation of synaptic NMDARs leads to PKC-dependent phosphorylation of RNF10 Ser31 and that this event plays a key role in *synapse-to-nucleus* associated signaling events. In particular, we

demonstrate that Ser31 phosphorylation drives CREB phosphorylation, transcription of RNF10 target genes and bidirectional modulation of dendritic spine density and neuronal branching. In particular, taking into account that CREB phosphorylation represents a highly validated molecular marker of NMDAR-dependent hippocampal LTP (18-24), the reduction of CREB phosphorylation observed in neurons transfected with Myc-RNF10Ser31Ala mutants confirms previous observations of our group showing an impairment of LTP following RNF10 silencing.

Overall these results indicate that PKC-dependent trafficking of RNF10 to the nucleus represents an essential element for the induction of NMDAR-dependent modulation of dendritic arborization and spine density in hippocampal neurons, indicating the novel synaptonuclear messenger RNF10 as a key player in the regulation of neuronal architecture. Interestingly, RNF10 KO mice are characterized by gross morphological alterations of the hippocampus as well as of several other brain regions (https://www.komp.org/geneinfo.php?geneid=77189; unpublished observations), thus suggesting a role of this protein not confined to the hippocampus.

ACKNOWLEDGMENTS

The authors are thankful to Anna Grassi, Francesco Tonolini and Marta Ornaghi for their technical support. DM is supported by DFG grants SFB1158 and FOR2325. DM is a member of the Excellence Cluster *Cell Networks* at Heidelberg University. This work was supported by the Italian Ministry of University and Research [PRIN 2015N4FKJ4 to MDL], Joint programme – Neurodegenerative disease research project STAD and by MIUR Progetto Eccellenza.

COMPETING INTERESTS

The authors declare that they have no competing interests.

REFERENCES

1. Fainzilber M, Budnik V, Segal RA, Kreutz MR (2011) From synapse to nucleus and back again--communication over distance within neurons. J Neurosci 31:16045-16048. https://doi.org/10.1523/JNEUROSCI.4006-11.2011.
2. Ch'Ng TH, Uzgil B, Lin P, Avliyakulov NK, O'Dell TJ, Martin KC (2012) Activity-dependent transport of the transcriptional coactivator CRTC1 from synapse to nucleus. Cell 150:207-221. https://doi.org/10.1016/j.cell.2012.05.027.
3. Herbst WA, Martin KC (2017) Regulated transport of signaling proteins from synapse to nucleus. Curr Opin Neurobiol 45:78-84. https://doi.org/10.1016/j.conb.2017.04.006.

4. Lim AFY, Lim WL, Ch'ng TH (2017) Activity-dependent synapse to nucleus signaling. Neurobiol Learn Mem 138:78-84. https://doi.org/10.1016/j.nlm.2016.07.024.
5. Karpova A, Mikhaylova M, Bera S, Bär J, Reddy PP, Behnisch T, Rankovic V, Spilker C, Bethge P, Sahin J, Kaushik R, Zuschratter W, Kähne T, Naumann M, Gundelfinger ED, Kreutz MR (2013) Encoding and transducing the synaptic or extrasynaptic origin of NMDA receptor signals to the nucleus. Cell 152:1119-1133. https://doi.org/10.1016/j.cell.2013.02.002.
6. Marcello E, Di Luca M, Gardoni F (2018) Synapse-to-nucleus communication: from developmental disorders to Alzheimer's disease. Curr Opin Neurobiol 48: 160-166 [2018]. https://doi.org/10.1016/j.conb.2017.12.017.
7. Dinamarca MC, Guzzetti F, Karpova A, Lim D, Mitro N, Musardo S, Mellone M, Marcello E, Stanic J, Samaddar T, Burguière A, Caldarelli A, Genazzani AA, Perroy J, Fagni L, Canonico PL, Kreutz MR, Gardoni F, Di Luca M (2016) Ring finger protein 10 is a novel synaptonuclear messenger encoding activation of NMDA receptors in hippocampus. Elife 5:e12430. https://doi.org/10.7554/eLife.12430.
8. Zheng X, Zhang L, Wang AP, Bennett MV, Zukin RS (1999) Protein kinase C potentiation of N-methyl-D-aspartate receptor activity is not mediated by phosphorylation of N-methyl-D-aspartate receptor subunits. Proc Natl Acad Sci USA 96:15262-15267.
9. Gardoni F, Schrama LH, Kamal A, Gispen WH, Cattabeni F, Di Luca M (2001) Hippocampal Synaptic Plasticity Involves Competition between Ca 2+/Calmodulin-Dependent Protein Kinase II and Postsynaptic Density 95 for Binding to the NR2A Subunit of the NMDA Receptor. J Neurosci 21:1501-1509.
10. Piccoli G, Verpelli C, Tonna N, Romorini S, Alessio M, Nairn AC, Bachi A, Sala C (2007) Proteomic analysis of activity-dependent synaptic plasticity in hippocampal neurons. J Proteome Res 6:3203-3215. https://doi.org/ 10.1021/pr0701308.
11. Paguio A, Almond B, Fan F, Stecha P, Garvin D, Wood M, Wood K (2005) pGL4 Vectors: A new generation of luciferase reporter vectors. Promega Notes 89
12. Otmakhov N, Khibnik L, Otmakhova N, Carpenter S, Riahi S, Asrican B, Lisman J (2004) Forskolin-induced LTP in the CA1 hippocampal region is NMDA receptor dependent. J Neurophysiol 91: 1955-1962
13. Toullec D, Pianetti P, Coste H, Bellevergue P, Grand-Perret T, Ajakane M, Baudet V, Boissin P, Boursier E, Loriolle F, Duhamel L, Charon D, Kirilovski J (1991) The bisindolylmaleimide GF 109203X is a potent and selective inhibitor of protein kinase C. J Biol Chem 1266:15771-15781.

14. Lin J, Friesen MT, Bocangel P, Cheung D, Rawszer K, Wigle JT (2005) Characterization of Mesenchyme Homeobox 2 (MEOX2) transcription factor binding to RING finger protein 10. Mol Cell Biochem 275:75-84.
15. Malik YS, Sheikh MA, Lai M, Cao R, Zhu X (2013) RING finger protein 10 regulates retinoic acid-induced neuronal differentiation and the cell cycle exit of P19 embryonic carcinoma cells. J Cell Biochem 114:2007-2015. https://doi.org/10.1002/jcb.24544.
16. Bajaj G, Hau AM, Hsu P, Gafken PR, Schimerlik MI, Ishmael JE (2014) Identification of an atypical calcium-dependent calmodulin binding site on the C-terminal domain of GluN2A. Biochem Biophys Res Commun 444:588-594. https://doi.org/10.1016/j.bbrc.2014.01.111.Robinson PJ (1992) Differential stimulation of protein kinase C activity by phorbol ester or calcium/phosphatidylserine in vitro and in intact synaptosomes. J Biol Chem 267:21637-21344.
17. Dash PK, Hochner B, Kandel ER (1990) Injection of the cAMP-responsive element into the nucleus of Aplysia sensory neurons blocks long-term facilitation. Nature 345:718-721.
18. Hardingham GE, Fukunaga Y, Bading H (2002) Extrasynaptic NMDARs oppose synaptic NMDARs by triggering CREB shut-off and cell death pathways. Nat Neurosci 5:405-414. https://doi.org/10.1038/nn835.
19. Sheng M, McFadden G, Greenberg ME (1990) Membrane depolarization and calcium induce c-fos transcription via phosphorylation of transcription factor CREB. Neuron 4:571-582.
20. Roberson ED, English JE, Adams JP, Selcher JC, Kondratick C, SweattJD (1999) The mitogen-activated protein kinase cascade couples PKA and PKC to cAM P response element binding protein phosphorylationin area CA1 of hippocampus. J Neurosci 19:4337– 4348.
21. Kanterewicz BI, Urban NN, McMahon DB, Norman ED, Giffen LJ, Favata MF, Scherle PA, Trzskos JM, Barrionuevo G, Klann E. The extracellular signal-regulated kinase cascade is required for NMDA receptor-independent LTP in area CA1 but not area CA3 of the hippocampus. J Neurosci. 2000 May 1;20(9):3057-66.
22. English JE, Sweatt JD (1997) A requirement for the mitogen-activatedprotein kinase cascade in hippocampal long-term potentiation. J BiolChem 272:19103–19106.
23. Hotte M, Thuault S, Dineley KT, Hemmings HC Jr, Nairn AC, Jay TM. Phosphorylation of CREB and DARPP-32 during late LTP at hippocampal to prefrontal cortex synapses in vivo. Synapse. 2007 Jan;61(1):24-8.
24. Spilker C, Nullmeier S, Grochowska KM, Schumacher A, Butnaru I, Macharadze T, Gomes GM, Yuanxiang P, Bayraktar G, Rodenstein C, Geiseler C, Kolodziej A, Lopez-Rojas J, Montag D,

Angenstein F, Bär J, D'Hanis W, Roskoden T, Mikhaylova M, Budinger E, Ohl FW, Stork O, Zenclussen AC, Karpova A, Schwegler H, Kreutz MR (2016) A Jacob/Nsmf gene knockout results in hippocampal dysplasia and impaired BDNF signaling in dendritogenesis. PLoS Genet 12: e1005907. https://doi.org/10.1371/journal.pgen.1005907.

25. Proepper C, Johannsen S, Siebau S, Dahl J, Vaida B, Bockmann J, Kreutz MR, Gundelfinger ED, Boeckers TM (2017) Abelson interacting protein 1 (Abi-1) is essential for dendrite morphogenesis and synapse formation. EMBO J 26:1397-1409. https://doi.org/10.1038/sj.emboj.7601569.
26. Finsterwald C, Fiumelli H, Cardinaux JR, Martin JL (2010) Regulation of dendritic development by BDNF requires activation of CRTC1 by glutamate. J Biol Chem 285:28587-28595. https://doi.org/10.1074/jbc.M110.125740.
27. Li S, Zhang C, Takemori H, Zhou Y, Xiong ZQ (2009) TORC1 regulates activity-dependent CREB-target gene transcription and dendritic growth of developing cortical neurons. J Neurosci 29:2334-2343. https://doi.org/10.1523/JNEUROSCI.2296-08.2009.
28. Li Z, Van Aelst L, Cline HT (2000) Rho GTPases regulate distinct aspects of dendritic arbor growth in Xenopus central neurons in vivo. Nat Neurosci 3:217-225. https://doi.org/10.1038/72920
29. Sin WC, Haas K, Ruthazer ES, Cline HT (2002) Dendrite growth increased by visual activity requires NMDA receptor and Rho GTPases. Nature 419:475-480. https://doi.org/10.1038/nature00987.
30. Mauceri D, Freitag HE, Oliveira AM, Bengtson CP, Bading H (2011) Nuclear calcium-VEGFD signaling controls maintenance of dendrite arborization necessary for memory formation. Neuron 71:117-130. https://doi.org/10.1016/j.neuron.2011.04.022.
31. Kuo TY, Chen CY, Hsueh YP (2010) Bcl11A/CTIP1 mediates the effect of the glutamate receptor on axon branching and dendrite outgrowth. J Neurochem 114:1381-1392. https://doi.org/10.1111/j.1471-4159.2010.06852.x.
32. Ewald RC, Van Keuren-Jensen KR, Aizenman CD, Cline HT (2008) Roles of NR2A and NR2B in the development of dendritic arbor morphology in vivo. J Neurosci 28:850-861. https://doi.org/10.1523/JNEUROSCI.5078-07.2008.
33. Kannangara TS, Bostrom CA, Ratzlaff A, Thompson L, Cater RM, Gil-Mohapel J, Christie BR (2014) Deletion of the NMDA receptor GluN2A subunit significantly decreases dendritic growth in maturing dentate granule neurons. PLoS One 9:e103155. https://doi.org/10.1371/journal.pone.0103155.

34. Balu D, Larson JR, Schmidt JV, Wirtshafter D, Yevtodiyenko A, Leonard AS (2016) Behavioral and physiological characterization of PKC-dependent phosphorylation in the Grin2aΔPKC mouse. Brain Res 1646: 15-326. https://doi.org/ 10.1016/j.brainres.2016.06.022.
35. Leonard AS, Hell JW (1997) Cyclic AMP-dependent protein kinase and protein kinase C phosphorylate N-methyl-D-aspartate receptors at different sites. J Biol Chem 272:12107-12115.
36. Lin Y, Jover-Mengual T, Wong J, Bennett MV, Zukin RS (2006) PSD-95 and PKC converge in regulating NMDA receptor trafficking and gating. Proc Natl Acad Sci USA 103:9902-19907. https://doi.org/ 10.1073/pnas.0609924104.
37. Shaner NC, Campbell RE, Steinbach PA, Giepmans BN, Palmer AE, Tsien RY (2004) Improved monomeric red, orange and yellow fluorescent proteins derived from Discosoma sp. red fluorescent protein. Nat biotechnol 22:1567-1572. https://doi.org/ 10.1038/nbt1037.

FIGURE CAPTIONS

Figure 1. Synaptic NMDAR stimulation induces RNF10 trafficking through PKC activation

a. In situ detection of proximity ligation assay (PLA) between RNF10 and GluN2A (red; left panels) along MAP2- (green; middle panels) in *DIV14* hippocampal neurons treated with vehicle (Ctr), SS (2,5 mM 4-AP and 50 μM Bicuculline for 30 minutes) or SS+BIM (preincubation with 10 μM BIM for 10 minutes, then SS). The histogram shows the quantification of the number of PLA clusters along MAP2-positive dendrites expressed as % of control. Scale bar: 10 μm

b. Representative confocal images and quantification of RNF10 (green) nuclear localization in hippocampal neurons treated at *DIV14* with vehicle, SS or SS+BIM. DAPI (blue) and PSD-95 (red, see merge panels) were used to stain nuclei and dendritic spines, respectively. The histogram shows the quantification of RNF10 integrated density (i.d.) in the nucleus expressed as % of control. Scale bar: 20 μm

c. Representative immunoblots and quantification of WB for RNF10 in nuclear extract from *DIV14* hippocampal neurons treated with vehicle, SS or SS+BIM. H3 was used as loading control. The histogram shows the quantification of RNF10 optical density (OD) normalized on Histone-H3 and expressed as % of control.

d. Representative immunoblots and quantification of WB for $p21^{WAF1/cip1}$ in nuclear extract from primary hippocampal neurons at DIV14 treated with vehicle, SS or SS+BIM. Tubulin was used as loading control. The histogram shows the quantification of $p21^{WAF1/cip1}$ optical density (OD) normalized on tubulin and expressed as % of control.

e. Representative confocal images and quantification of RNF10 (green) nuclear localization in hippocampal neurons treated at *DIV14* with vehicle or 10 μM PMA for 15 minutes. DAPI (blue) and PSD-95 (red) were used to stain nuclei and dendritic spines, respectively. The histogram shows the quantification of RNF10 integrated density (i.d.) in the nucleus expressed as % of control (ctr). Scale bar: 20 μm

f. Representative immunoblots and quantification of WB for RNF10 in nuclear extract from *DIV14* hippocampal neurons treated with vehicle or PMA. The histogram shows the quantification of RNF10 optical density (OD) normalized on Histone-H3 and expressed as % of control.

Statistical analysis: One-way ANOVA; *p<0.05, **p<0.01, ***p<0.001 (vs Ctr); #p<0.05, ##p<0.01 (vs SS+BIM).

Figure 2. PKC dependent phosphorylation on Ser31.

a. Representative immunoblots and quantification of an immunoprecipitation (IP) experiment on homogenates of *DIV14* hippocampal neurons treated with vehicle, SS or SS+BIM. Phospho-Ser proteins were immunoprecipitated and RNF10 revealed by western blotting in the immunoprecipitated material. The histogram shows the quantification of the phosphorylated RNF10 (pRNF10) optical density (OD) expressed as % of control.

b. GST and GST-RNF10WT, GST-RNF10S5D, GST-RNF10S31D, GST-RNF10S39D, GST-RNF10S70D fusion proteins were incubated in a pull-down assay with rat hippocampal extracts. GluN2A was revealed by western blotting analysis. The histogram shows the quantification of GluN2A optical density (OD) expressed as % of pull-down assay performed with RNF10WT.

c. Representative immunoblots and quantification of Co-IP experiment on homogenates of COS-7 cells transfected with Myc-RNF10WT, Myc-RNF10S31D or Myc-RNF10S31A. GluN2A was immunoprecipitated and RNF10 revealed. GluN2A was used as loading control. The histogram shows the quantification of RNF10 interaction with GluN2A (RNF10/GluN2A optical density, OD) expressed as % of the sample transfected with RNF10WT.

d. Representative immunoblots and quantification of western blotting for PSer31-RNF10, RNF10 and tubulin in Triton Insoluble Fractions of primary hippocampal neurons treated at *DIV14* with vehicle, SS or SS+BIM. Tubulin was used as loading control. The histogram shows the quantification of PSer31-RNF10/RNF10 ratio optical density (OD) after normalization on tubulin and expressed as % of control.

e. Representative immunoblots and quantification of western blotting for PSer31-RNF10, RNF10 and tubulin in Triton Insoluble Fractions of primary hippocampal neurons treated at *DIV14* with vehicle

or cLTP. Tubulin was used as loading control. The histogram shows the quantification of PSer31-RNF10/RNF10 ratio optical density (OD) after normalization on tubulin and expressed as % of control

f. Representative immunoblots and quantification of western blotting for PSer31-RNF10, RNF10 and H3 in crude nuclear fractions of primary hippocampal neurons treated at *DIV14* with vehicle (Ctr) or SS protocol. H3 was used as loading control. The histograms show the quantification of PSer31-RNF10 optical density (OD) after normalization on H3 (left graph) or on total RNF10 (right graph) and expressed as % of control.

g. In situ detection of PLA assay with RNF10S31P and total RNF10 antibodies (red; left panels) in the nucleus (DAPI, blue) in *DIV14* hippocampal neurons treated with vehicle (Ctr) or SS protocol. Map2 staining is shown in green. The histogram shows the quantification of the number of nuclear PLA clusters. Scale bar: 10 µm.

Statistical Analysis: (a-d) One-way ANOVA; *p<0.05, **p<0.01 (vs Ctr); #p<0.05 (vs RNF10S31D), ##p<0.01 (vs SS+BIM); (e-g) Student T-test; *p<0.05, ***p<0.001 (vs, Ctr).

Fig 3 PKC dependent phosphorylation on Ser31 modulates RNF10 trafficking

a. Synaptic stimulation treatment induces RNF10WT-tdEOS but not RNF10S31A-tdEOS translocation from distal dendrites to the nucleus in hippocampal neurons. Left panels: baseline confocal image of RNF10WT-tdEOS and RNF10S31A-tdEOS expressing hippocampal neuron illuminated sequentially with 488 nm (green panels) and 555 nm laser excitation wavelengths showing no emitted signal in the red spectra (0 min panels). Distal dendrite selected for photoconversion was illuminated with UV laser (405 nm wavelengths) repetitively through the image z-stack. Right panels: depicted are confocal max intensity projection images at respective time points (6, 12, 18, 24 and 30 minutes) after synaptic stimulation protocol. The histogram shows a significant increase in RNF10WT-tdEOS but not RNF10S31A-tdEOS photoconverted fluorescent intensities (red) in the nucleus following synaptic stimulation protocol. Scale bar: 30 µm

b. Representative confocal images and quantification of PLA (GluN2A/Myc-RNF10 interaction; red, upper panels) in *DIV14* primary hippocampal neurons transfected with Myc-RNF10WT or Myc-RNF10S31D. The histogram shows the quantification of PLA clusters along GFP-positive dendrites expressed as number of clusters in 10 µm of dendrite. PLA clusters outside GFP-positive dendrites were not considered for the quantification. Scale bar: 20 µm

c. Representative confocal images and quantification of Myc-RNF10 (green) nuclear localization in primary hippocampal neurons at DIV14 transfected with Myc-RNF10WT or Myc-RNF10S31D. DAPI (blue) was used to stain nuclei. The histogram shows the quantification of Myc-RNF10 integrated density in the nucleus expressed as % of Myc-RNF10WT. Scale bar: 15 μm

d. Histogram showing the quantification of Luciferase assay performed on lysates of neurons in which the p21prom-Luc2-T2A-tdTomato reporter plasmid was co-transfected in primary hippocampal neurons with a plasmid containing an expression cassette for *Renilla* luciferase for normalization with or without either RNF10WT, RNF10S31D or RNF31S31A.

Statistical Analysis: (c) One-way ANOVA; *p<0.05, **p<0.01 (vs Ctr); #p<0.05 (vs RNF10S31D), ##p<0.01 (vs SS+BIM). (a,b,d) Student T-test; ***p<0.001.

Figure 4. Modulation of RNF10 levels or activity affects neuronal morphology

a. Representative confocal images and quantification of pCREB (green) levels in *DIV14* hippocampal neurons transfected with Myc-RNF10WT, Myc-RNF10S31A or Myc-RNF31S31D. DAPI (blue) was used to stain nuclei. Transfected neurons were recognized with anti-Myc antibody (red). The histogram shows the quantification of pCREB integrated density (i.d.) in the nucleus expressed as % of control. Scale bar: 10 μm

b. Representative confocal images and quantification of dendritic spine density in *DIV14* hippocampal neurons transfected with GFP alone (upper panel) or co-transfected with GFP and Myc-RNF10WT, Myc-RNF10S31A or Myc-RNF31S31D. The histogram shows the quantification of dendritic spine density expressed as number of spines in 10 μm of dendrite. Scale bar: 5 μm

c. Representative confocal images (left panels) and Sholl analysis (right graph) of *DIV14* hippocampal neurons transfected with scr-RNF10, sh-RNF10 or controls. The histogram in the middle shows the quantification of total dendritic length. Scale bar: 40 μm

d. Representative confocal images (left panels) and Sholl analysis (right graph) of *DIV14* hippocampal neurons transfected with Myc-RNF10WT, Myc-RNF10S31A or Myc-RNF31S31D. The histogram in the middle shows the quantification of total dendritic length. Scale bar: 40 μm

Statistical Analysis: One-way ANOVA; *p<0.05, **p<0.01, ***p<0.001 (vs Ctrl); #p<0.05 (vs Myc-RNF10WT), ##p<0.01 (vs scr-RNF10), ###p<0.001 (vs Myc-RNF10S31D); $p<0.05 (vs Myc-RNF10S31D).

Figure 1

Click here to access/download;Figure;figure1r.jpg

FIGURE 1

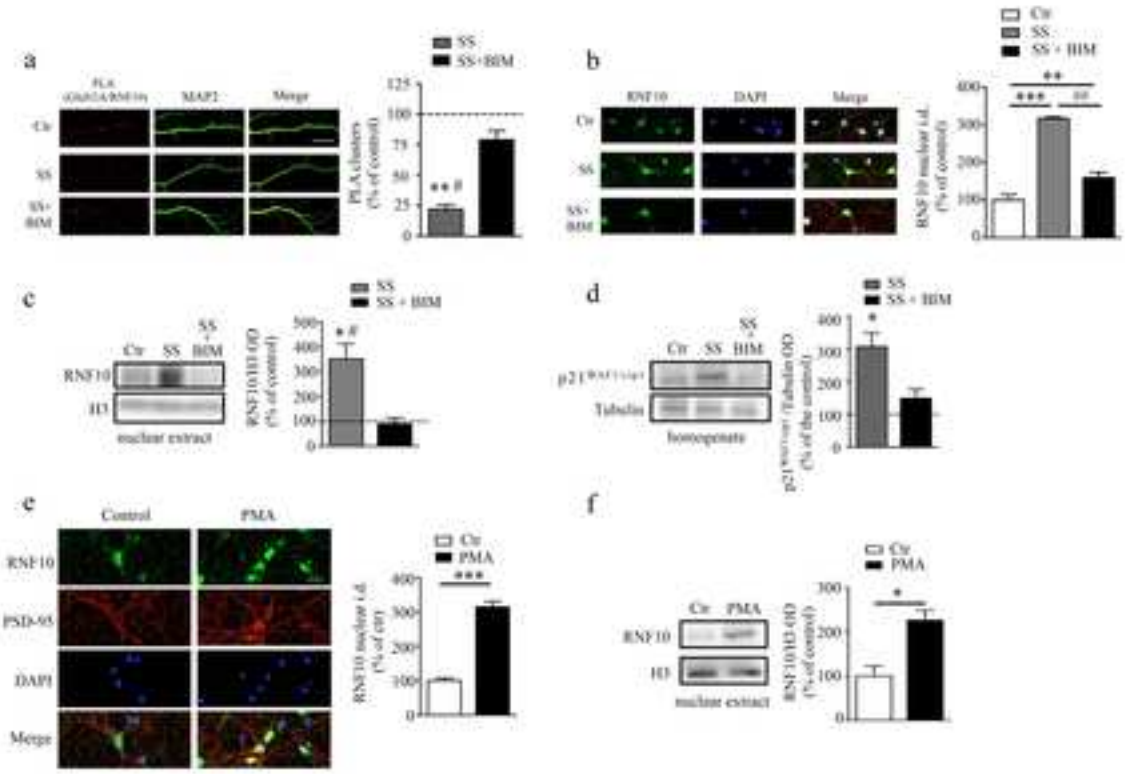

Figure 2

Click here to access/download;Figure;figure2r.jpg

FIGURE 2

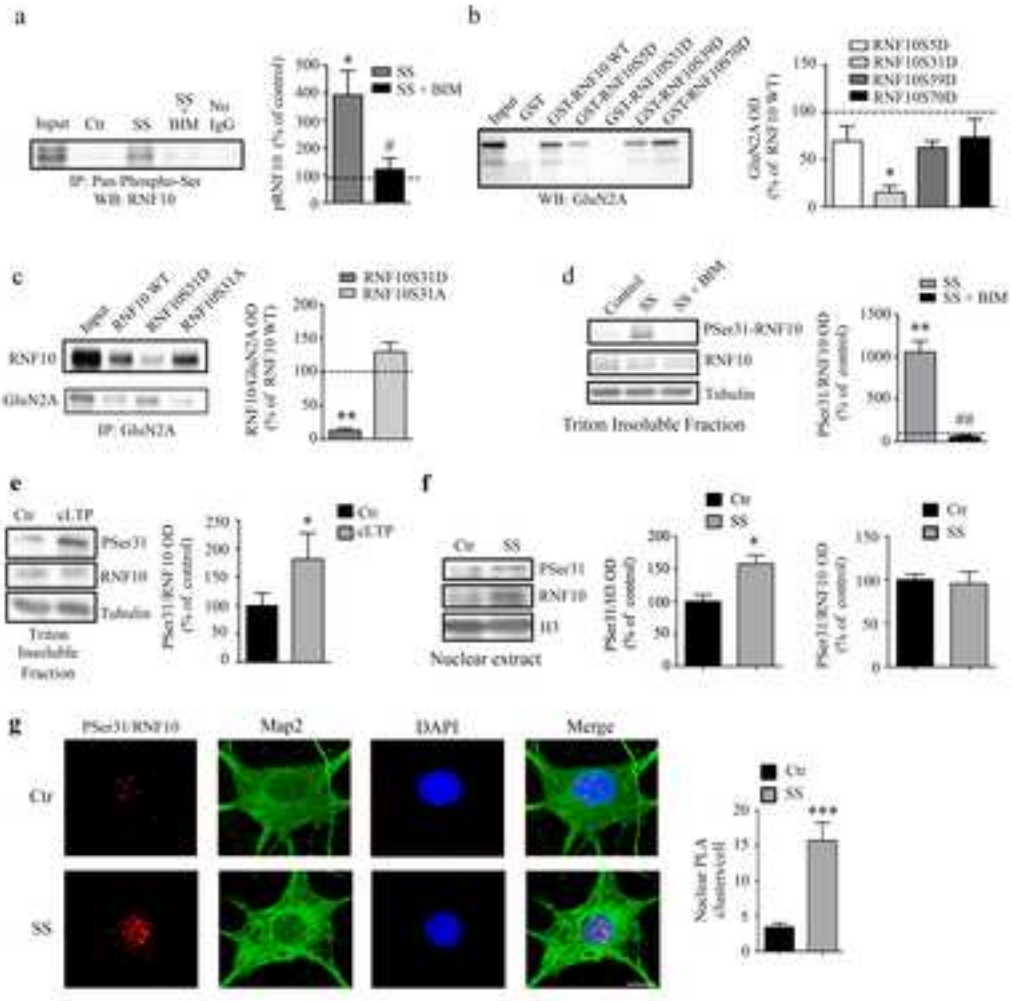

Figure 3

Click here to access/download;Figure;figure3r.jpg

FIGURE 3

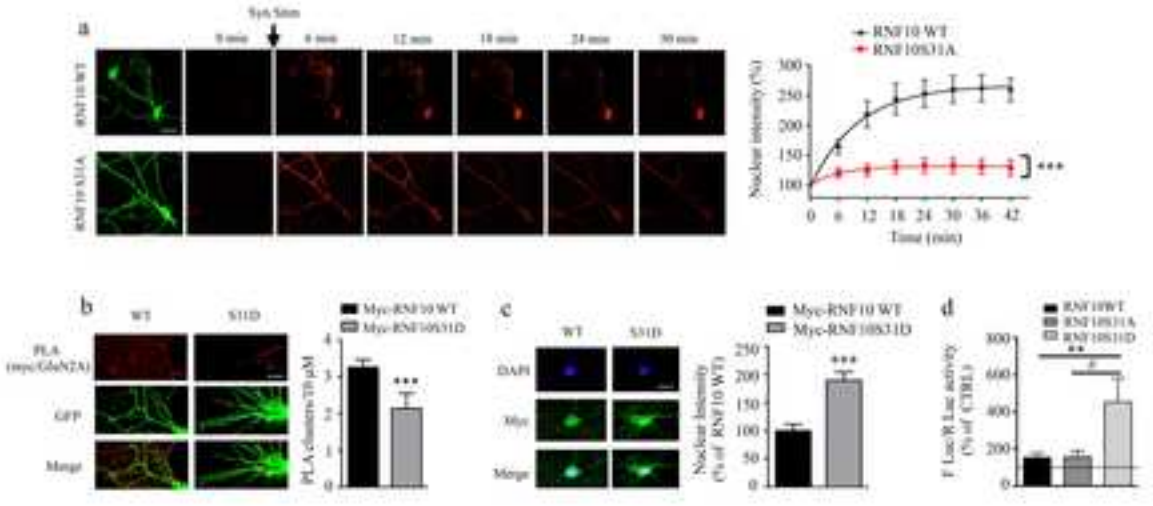

FIGURE 4